Multi-Scale Image Fusion Scheme based on Gray-Level Edge Maps and Adaptive Weight Maps

Jitesh Pradhan, Ankesh Raj, Arup Kumar Pal, and Haider Banka

Dept. of Computer Science and Engineering
Indian Institute of Technology (ISM) Dhanbad-826004, INDIA
jitpradhan02@gmail.com, ankesh.1200@gmail.com, arupkrpal@gmail.com, and haider.banka@gmail.com

Abstract. Digital cameras and other digital devices can not focus on all significant objects within the single frame due to their limited depth-of-focus. Consequently, few objects get attention in the captured image while rest of the objects becomes background information. This problem can be overcome using different multi-focus image fusion techniques because it combines all the partially focused objects of different parent images into a single fully focused fused image. Hence, the final fused image focuses on each and every object of the parent images. In this paper, a novel multi-focus image fusion technique has been proposed which uses different edge finding operators (like Sobel, Prewitt, Roberts and Scharr) on pre-processed images. These different edge finding operators have great pixel discrimination property which helps us to locate all the vital textural information of different partially focused images. Subsequently, an adaptive weight calculation approach has been introduced to generate weight maps of different parent images. Finally, all these parent image weight maps have been deployed into the winner-take-all scheme to integrate all parent images into a single fused image. Further, we have also considered different sets of partially focused images for experimental analysis. The experimental outcomes reveal that the proposed scheme is outperforming as compared to recent state-of-arts.

Keywords: Adaptive weight maps · Depth-of-focus · Edge maps · Image fusion · Multi-focus.

1 Introduction

1.1 Background

The human brain has capability to simulate very complex calculations within fraction of second which helps our visual system to focus different depth-of-field (DoF) objects simultaneously. Consequently, the discrimination power of human visual system is highly enhanced to see all salient objects of a single scene with very high clarity. But in digital devices the different DoF can be achieved by

adjusting different camera settings to focus on different objects of the same scene. As a result, only single object can be focused by a typical single lens digital camera. The object which has similar DoF with respect to the digital camera will be focused and the remaining part of image will be considered as background information. Hence, it is required to capture multiple images with different DoF settings of digital camera to capture all prominent objects of the same scene. The major overhead with this approach is the processing of large number of images which exceedingly increases the storage space along with the transmission bandwidth. To address all these issues, multi-focus image fusion scheme [1] has been deployed. In this multi-focus image fusion process, multiple partially focused parent images of a single scene have combined together to generate a highly enhanced fused image which replicates the effect of human visual system. Thus, the final fused image binds all the salient focused regions of different parent images into a single frame. The multi-focus image fusion techniques are very useful in the field of medical imaging, robotics, military, machine vision, photography and remote sensing. Hence, in todays scenario a highly precise and efficient multi-focus image fusion scheme is required to address all these key challenges.

1.2 Literature Review

At the present time, the different multi-focus image fusion schemes can be categorized into two classes which are spatial and transformed domain based schemes [2]. Here, spatial domain schemes directly use linear combination image fusion approaches into the source parent images. Generally, all these spatial domain schemes use either pixel based or block based fusion techniques. Pixel based techniques considers each and every pixel of the parent image and perform averaging operation for image fusion process. Consequently, these methods often fall under misregistration and noise problems. All these overheads can be controlled by considering block based approaches rather than pixel based approaches because the importance of every pixel where defined with the help of its neighborhood pixels. Initially, Goshtasy et al. [3] have addressed the image registration problem in the multi-focus image fusion scheme. They have registered all partially focused images into similar frame size and employed uniform non-overlapping block-division fusion scheme. Further, they have integrated the blocks of different parent images which have higher gradient average into final fused image. In 2007, Huang et al. [4] have also addressed image registration problem by considering the performance of sharpness matrices. Piella et al. [5] have used saliency factors of different image regions for image fusion. They have performed uniform block division and considered the degree of saliency of each block for image fusion process. Luo et al. [6] have introduced a new multi-focus image fusion scheme which follows the region partition tactics. This scheme removes the redundant regions of the parent images by considering the region homogeneity components. Some contemporary researchers have also proposed several transform domain based image fusion schemes. Here, Li et al. [7] have introduced a transform domain based multi-focus image fusion scheme which uses

combination of curvelet and wavelet transforms. Further, in 2009 Looney et al. [8] have introduced a novel image fusion scheme which was inspired from the data driven strategies. This data driven scheme decomposes the image signals into original scale components. In particular, this technique has been called as Empirical mode decomposition (EMD). Later, Nejati et al. [9] have proposed a new focus creation scheme based on the surface area of the different intersection regions of parent images. In this scheme, all input images have been segmented based on the extracted intersection points. Afterwards, they have performed the images fusion process based on the surface area of different regions. In 2017, Luo et al. [1] have used edge intensity (EDI) values along with higher order singular value decomposition (HOSVD) for multi-scale image fusion. In their scheme, they have used EDI to measure the edge sharpness and HOSVD to decompose the parent images. Finally, they have employed a sigmoid function to perform the image fusion task.

1.3 Motivation and Contribution

Generally, all natural images possess rich textural information, clear and sharp edges along with definite boundaries. Thus the focused region of any image will have more detailed and sharp edges and boundaries. All these localized image information can be easily extracted by applying different transformation tools along with image decomposition approaches. But, this combination of image decomposition and transformation increases the time overhead and complexity of the image fusion process. These additional overheads can be controlled by applying different spatial domain techniques. In this paper, we have used different edge detection operators to enhance and extract the local geometrical structures of the image. In this paper, our main contributions are as follows:

- Point matching image registration technique has been adopted to produce identical frame images of all partially focused parent images.
- Non-linear anisotropic diffusion method has been employed on parent images to eliminate all possible noise.
- Different edge finding operators have been used to emphasize the local geometrical structure of the partially focused parent images.
- An adaptive weight calculation scheme has been introduced to calculate the importance of each parent image.
- Weight map based winner-take-all approach has been proposed for final image fusion process.

2 Basic building blocks

2.1 Non-linear anisotropic diffusion (NLAD)

In general, most of the images possess homogeneous and non-homogeneous pixel regions. The image regions where group of pixels shows similar behaviors are treated as homogeneous pixel region. Subsequently, those pixel regions which

show huge diversity in their characteristics are treated as non-homogeneous pixel regions. Here, a partial differential equation (PDE) has been employed in anisotropic diffusion to enhance the non-homogeneous pixel regions. This approach not only preserves the non-homogeneous pixel regions but also perform region smoothening operation. In this work, we have adopted the non-linear anisotropic diffusion [10] scheme to eliminate the noise factors from the partially focused images. This NLAD scheme is efficient and robust since it considers the non-homogeneous pixel regions. This scheme computes a flux function to control the diffusion of parent images. For any image P, NALD flux function has been defined as follows:

$$f(i,j,t) = df(\delta|P(i,j,t)|) \tag{1}$$

Here, flux function or rate of diffusion has been represent by f. Further, gradient operator and number of iteration/scale/time have been represented by δ and t respectively. At the same time, diffusion function df is defined as follows:

$$df(|X|) = e^{-\{|X|/C\}^2} \tag{2}$$

$$df(|X|) = \left(\frac{1}{1+(|X|/C)^2}\right) \tag{3}$$

Diffusion function has been defined in two different ways and these functions have capability to create trade-off between homogeneous region smoothening and edge preservation. If any image possess more sharp boundaries than first function will be very useful whereas second function will be more useful for images with wide regions. Here, C is a free parameter which helps to validate the clear boundaries of different image regions. Fig.1 shows the output of NLAD process and in this fig. 1 we can see that the noise has been efficiently removed.

Fig. 1. (a) Noisy cameraman image, (b) Output noise free cameraman image (c) Noisy texture image and (d) Output noise free texture image.

2.2 Edge detection

In different vision systems, edge detection [11] plays a critical role since it gives local information of different geometrical structures, T junctions, straight lines

and textural patterns. Edge detection is very useful in image fusion, segmentation, object detection and object tracking. In general, different edges can be detected by analyzing the variations along x-axis and y-axis gradients. These gradients can be computes with the help of different edge kernels. In this paper we have used Sobel, Prewitt, Robert, and Scharr edge kernels to detect edges. Later, fig. 2 demonstrates the simple schematic diagram of edge detection process.

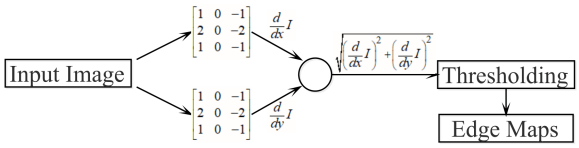

Fig. 2. Schematic diagram of simple edge detection process.

3 Proposed multi-focused image fusion scheme

A new multi-focused image fusion scheme has been introduced in this paper which uses edge maps and adaptive weight maps of different parent image for image integration. In this scheme, n different partially focused parent images have been selected. All these parent images have been captured at different DoF for a single scene. Suppose, $P_1, P_2, P_3, ..., P_n$ represent the n different partially focused parent images and all these images have been used as input images. First, we have employed Point Matching Image Registration technique on all input images. This technique will transforms all these images into a similar image frame or coordinate system. In the next step, we have generated the gray-scale images of all registered parent images i.e. $Pg_1, Pg_2, Pg_3, ..., Pg_n$. Many times it has been observed that these gray-scale images possess high noise factor which ultimately affects the quality of image integration. Hence, to avoid this problem we have used non-linear anisotropic diffusion (NLAD) scheme in gray-scale parent images. This NLAD scheme not only removes the noise but also elevates the visually salient features of the any image. All these noise free images have been represented as $Pf_1, Pf_2, Pf_3, ..., Pf_n$. Next, we have used different edge detection kernels to enhance and detect all local geometrical structures and boundaries of the parent images. This process will generate a detailed gray-scale edge map for every noise free image i.e. $Pe_1, Pe_2, Pe_3, ..., Pe_n$. Finally, we have used proposed weight map calculation scheme along with winner-take-all approach to integrate all parent images into a single fully focused image. In the following sub-section we have discussed this proposed image integration scheme in detailed.

3.1 Adaptive weight map calculation

Adaptive weight map Pw of any parent image gray-scale edge map Pe shows the significance of each and every pixel in its surroundings. Those pixels which lie in the focused area will have higher weights in the weight map. These weight maps will be used for final image fusion process. We have selected different neighborhood window size for every pixel of the gray-scale edge map to calculate their weights. Here, weight of any pixel reflects the uniqueness of the pixel in its surroundings. In the experiments we have considered 3×3, 5×5, 7×7, 9×9 and 11×11 neighborhood window size for weight map calculation and for image integration. Here we will discuss how an $m \times m$ neighborhood window size based weight map for $n \times n$ gray-scale edge map has been calculated where $m < n$.

First we have considered a gray-scale edge map Pe_j of the j^{th} parent image P_j. For any pixel $Pe_j(x, y)$ we have extracted the $m \times m$ size neighborhood window. In this window the center pixel will be the $Pe_j(x, y)$. Let Nw_i represents the $m \times m$ size neighborhood window for the i^{th} pixel P_c of a gray-scale edge map Pe_j. Further, we have extracted the different neighborhood levels with respect to the center pixel P_c of Nw_i. For an $m \times m$ window, there will $(m-1)/2$ neighborhood levels. The immediate neighborhood pixels of the center pixel will fall under level 1 and the last pixels of the window will fall under the $(m-1)/2$ level. Fig. 3, shows the 9×9 neighborhood representation for the i^{th} pixel P_c of a given edge map Pe_j. In the above figure, the center pixel P_c is the i_{th} pixel

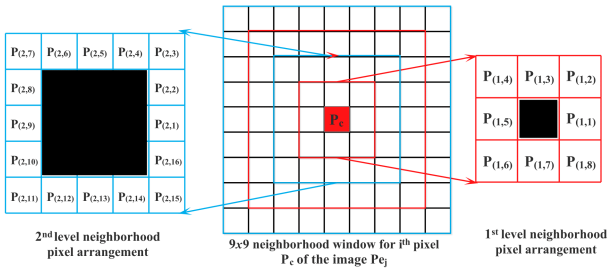

Fig. 3. 9×9 neighborhood representation for the i^{th} pixel P_c of a given edge map Pe_j.

of the image and its weight W_c in $m \times m$ size neighborhood window will be calculated as follows:

$$W_c = \frac{1}{2} \times P_c + \frac{1}{2} \sum_{k=1}^{(m-1)/2} w_k \tag{4}$$

Here, w_k represents the relative weight value of the k^{th} neighborhood level which is defined as follows:

$$\mu_k = \frac{1}{N} \times \sum_{l=1}^{N} P_{(k,l)} \tag{5}$$

$$d_k = P_c - \mu_k \tag{6}$$

$$w_k = \frac{d_k}{\sum_{r=1}^{(m-1)/2} d_r} \tag{7}$$

Here, N is the number of pixels falls under k^{th} neighborhood level and P_c gives the intensity value of the center pixel. $P_{(k,l)}$ is the intensity value of the l^{th} pixel of k^{th} neighborhood level. In this way an adaptive weight map Pw_j will be generated for given gray-scale edge map Pe_j.

3.2 Winner-take-all scheme

In this step, we will select all the partially focused parent images $P_1, P_2, P_3, ..., P_n$ as well as their weight maps $Pw_1, Pw_2, Pw_3, ..., Pw_n$. These original maps and weight maps will be used for the final image integration process. First, we will select the i^{th} pixel from each partially focused parent image with their corresponding weight values from the weight maps. The i^{th} pixel of any image which has maximum weight value will be the winner pixel and will be integrated in the final fully focused image. The final fully focused fused image F_f is calculated as follows:

$$F_f^C(x,y) = \begin{cases} F_f^C(x,y) = P_1^C(x,y), & \text{If } fw(Pw_i(x,y)) = Pw_1(x,y) \\ F_f^C(x,y) = P_2^C(x,y), & \text{If } fw(Pw_i(x,y)) = Pw_2(x,y) \\ F_f^C(x,y) = P_3^C(x,y), & \text{If } fw(Pw_i(x,y)) = Pw_3(x,y) \\ ... & \\ F_f^C(x,y) = P_i^C(x,y), & \text{If } fw(Pw_i(x,y)) = Pw_i(x,y) \\ ... & \\ F_f^C(x,y) = P_n^C(x,y), & \text{If } fw(Pw_i(x,y)) = Pw_n(x,y) \end{cases} \tag{8}$$

Here, $F_f^C(x,y)$ represents the i^{th} pixel of the different color components of the final image F_f where, $C \in \{Red, Green, Blue\}$ color components. So, i^{th} pixel of different color components will be written as $F_f^{Red}(x,y)$, $F_f^{Green}(x,y)$ and $F_f^{Blue}(x,y)$. Similarly, $P_i^C(x,y)$ represents the i^{th} pixel of the different color components of any parent image P_i. Simultaneously, $fw(.)$ is the winner function and it is defined as follows:

$$fw(Pw_i(x,y)) = maxof\left\{Pw_1(x,y), Pw_2(x,y), Pw_3(x,y), ..., Pw_n(x,y)\right\} \tag{9}$$

3.3 Proposed multi-focused image fusion architecture

Algorithm 1 shows the different steps of the proposed multi-focus image integration scheme. Subsequently, the schematic block diagram of the suggested image integration scheme has been shown in fig. 4.

Algorithm 1 Multi-scale Image Fusion.

Input: n partially focused parent images i.e. $P_1, P_2, P_3, ..., P_n$.
Output: Final fully focused integrated image F_f.

1: Select n partially focused parent images $P_1, P_2, P_3, ..., P_n$ of the same scene with different DOF.
2: Use Point Matching Image Registration technique to transform all parent images to achieve identical frame structure..
3: Compute gray-scale images $Pg_1, Pg_2, Pg_3, ..., Pg_n$ of all registered images.
4: Generate the noise free images $Pf_1, Pf_2, Pf_3, ..., Pf_n$ by employing non-linear anisotropic diffusion (NLAD) in all gray-scale parent images.
5: Apply Sobel, Prewitt, Robert, or Scharr edge kernels in all noise free images to generate gray-scale parent edge maps $Pe_1, Pe_2, Pe_3, ..., Pe_n$.
6: Apply $m \times m$ neighborhood adaptive weight map calculation technique to generate weight maps $Pw_1, Pw_2, Pw_3, ..., Pw_n$ of all gray-scale edge maps.
7: Select all n weight maps $Pw_1, Pw_2, Pw_3, ..., Pw_n$ and original parent images $P_1, P_2, P_3, ..., P_n$ for winner-take-all scheme to integrate all important pixels of different parent images into single fully focused image F_f.

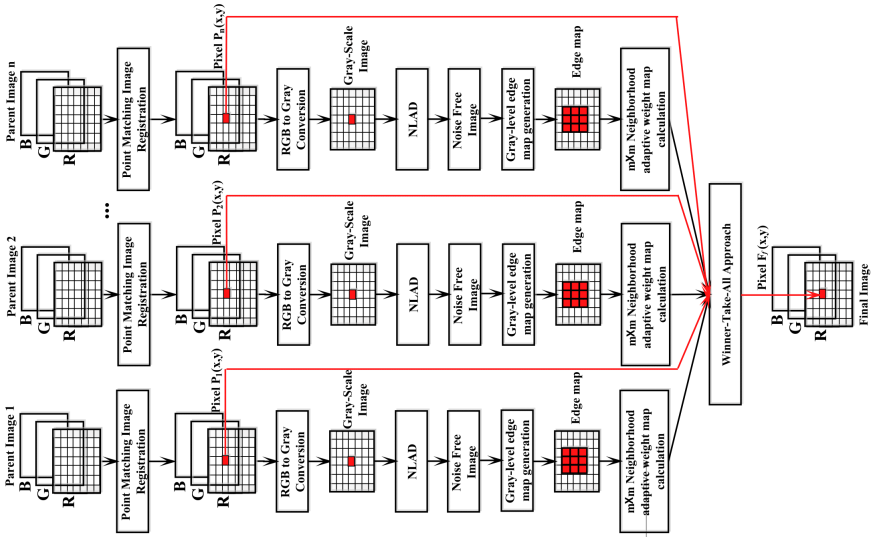

Fig. 4. Schematic block diagram of the proposed multi-scale image integration scheme.

4 Experimental Results and Discussion

In this paper, we have conducted several image fusion experiments on 2 different partially focused image datasets. These image datasets are standard image sets which are widely used in image fusion experiments. These datasets are Book and Clock image datasets. In these datasets two different focused images with their resultant fused image are present for comparative analysis. We have employed

Sobel, Prewitt, Robert, and Scharr edge kernels in all image sets in the experiments. Fig. 5 shows the output gray-scale edge maps for different Book images. We have carried out our first image fusion experiment on Book image dataset which contains two partially focused and one reference image of size 1024×768. We have used 3×3 neighborhood window for adaptive weight map generation along with all 4 edge detection kernels. The output of the image fusion process on this Book dataset has been shown in fig. 6.

Fig. 5. Output different gray-scale edge maps for different Book images.

Fig. 6. Image fusion results on Book image set (a) Parent image 1 (b) Parent image 2 (c) Reference image (d) Sobel output (e) Prewitt output (f) Roberts output (d) Scharr output.

In this Book image dataset fusion experiments, we have also considered different neighborhood windows for adaptive weight map calculation. Further, we have used these different adaptive weight maps with different edge kernels for fusion experiments. Here, we have calculated peak signal to noise ratio (PSNR), Structural Similarity (SSIM) and root mean square error (RMSE) to check the performance of image fusion. Table 1 to 4 shows the experimental results of all these image fusion experiments on Book image set. Next, we have carried out our second on Clock image dataset which contains two partially focused and one reference image of size 512×512. The output integrated images generated from these experiments have been presented in figure 7. Later, table 5 to 8 shows

the experimental results of all these image fusion experiments on Clock image dataset.

Table 1. Image fusion performance on Book image dataset using Sobel kernels.

Performance Parameter	**Different neighborhood window size for adaptive weight map calculation**				
	3×3	5×5	7×7	9×9	11×11
PSNR	27.7930	26.6628	25.6663	24.8803	24.2065
RMSE	0.0411	0.0464	0.0521	0.0570	0.0616
SSIM	0.9466	0.9453	0.9441	0.9438	0.9436

Table 2. Image fusion performance on Book image dataset using Prewitt kernels.

Performance Parameter	**Different neighborhood window size for adaptive weight map calculation**				
	3×3	5×5	7×7	9×9	11×11
PSNR	27.7436	26.6666	25.6654	24.8698	24.2098
RMSE	0.0410	0.0464	0.0521	0.0571	0.0612
SSIM	0.9471	0.9454	0.9442	0.9437	0.9435

Table 3. Image fusion performance on Book image dataset using Robert's kernels.

Performance Parameter	**Different neighborhood window size for adaptive weight map calculation**				
	3×3	5×5	7×7	9×9	11×11
PSNR	27.7597	26.7356	25.7679	24.9607	24.2779
RMSE	0.0409	0.0460	0.0515	0.0565	0.0611
SSIM	0.9473	0.9463	0.9463	0.9461	0.9457

Table 4. Image fusion performance on Book image dataset using Scharr kernels.

Performance Parameter	**Different neighborhood window size for adaptive weight map calculation**				
	3×3	5×5	7×7	9×9	11×11
PSNR	27.7044	26.6684	25.6735	24.8862	24.2094
RMSE	0.0412	0.0464	0.0520	0.0570	0.0616
SSIM	0.9465	0.9453	0.09441	0.09441	0.09441

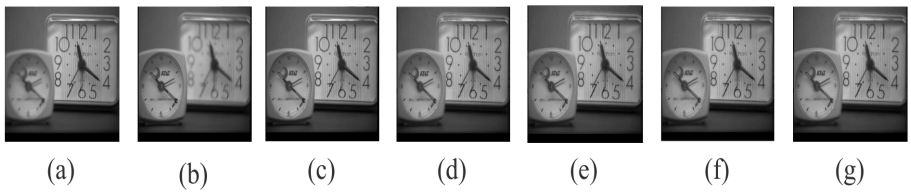

Fig. 7. Image fusion results on Clock image set (a) Parent image 1 (b) Parent image 2 (c) Reference image (d) Sobel output (e) Prewitt output (f) Roberts output (d) Scharr output.

Table 5. Image fusion performance on Clock image dataset using Sobel kernels.

Performance Parameter	**Different neighborhood window size for adaptive weight map calculation**				
	3×3	5×5	7×7	9×9	11×11
PSNR	30.9533	32.8023	33.6181	33.9233	33.2724
RMSE	0.0283	0.0229	0.0208	0.0201	0.0202
SSIM	0.9366	0.9395	0.9419	0.9423	0.9419

Table 6. Image fusion performance on Clock image dataset using Prewitt kernels

Performance Parameter	**Different neighborhood window size for adaptive weight map calculation**				
	3×3	5×5	7×7	9×9	11×11
PSNR	30.9500	32.7623	33.6412	33.8807	33.8861
RMSE	0.0283	0.0230	0.0208	0.0202	0.0202
SSIM	0.9368	0.9396	0.9421	0.9424	0.9423

Table 7. Image fusion performance on Clock image dataset using Roberts kernels.

Performance Parameter	**Different neighborhood window size for adaptive weight map calculation**				
	3×3	5×5	7×7	9×9	11×11
PSNR	30.5863	32.1903	33.0665	33.7695	33.8801
RMSE	0.0296	0.0246	0.0222	0.0205	0.0202
SSIM	0.9277	0.9315	0.9353	0.9372	0.9386

Table 8. Image fusion performance on Clock image dataset using Scharr kernels.

Performance Parameter	**Different neighborhood window size for adaptive weight map calculation**				
	3×3	5×5	7×7	9×9	11×11
PSNR	30.9394	32.7662	33.6152	33.9159	33.8922
RMSE	0.0284	0.0230	0.0209	0.0201	0.0202
SSIM	0.9362	0.9388	0.9414	0.9423	0.9418

Further, we have also compared our proposed multi-scale image fusion scheme with other standard image fusion schemes. These are curvelet transform, morphological component analysis (MCA), discrete cosine transform (DCT), TV-11 model and block-level DCT based image fusion schemes. Here, table 9 demonstrates the comparative analysis in terms of PSNR and execution time for Book image dataset. We have calculated these results by comparing the reference Book image with the output fused Book image.

Table 9. PSNR and Execution time performance analysis between different multi-scale image fusion techniques and the proposed image fusion technique.

S. No.	**Schemes**	**PSNR**	**Execution Time**
1.	**MCA**	27.7943	6.8715 sec.
2.	**DCT**	22.4146	1.9588 sec.
3.	**Block DCT**	25.5751	5.3015 sec.
4.	**TV**	21.7943	6.5781 sec.
5.	**Curvelet**	25.2725	1.6655 sec.
6.	**Proposed**	27.7930	6.7821 sec.

Table 10. Different evolution parameter based performance comparisons between current multi-scale image fusion techniques and the proposed image fusion technique.

S.No.	Method	RW	SSIM	FD	MI	QAB/F
1.	**MCA**	0.0408	0.8977	7.1332	4.3807	0.6329
2.	**TV-l1**	0.1928	0.7931	12.5483	3.8879	0.6386
3.	**LP**	0.0062	0.9211	11.6845	5.2433	0.7746
4.	**RP**	0.0097	0.9436	10.0131	5.6569	0.7625
5.	**MP**	0.0177	0.09048	12.1859	4.4438	0.7296
6.	**GP**	0.0862	0.8954	10.4233	4.0176	0.7416
7.	**FSD**	0.0861	0.8927	10.4930	4.0011	0.7310
8.	**DWT**	0.0033	0.9136	12.3349	4.8076	0.7621
9.	**CP**	0.0087	0.9168	11.9958	5.3669	0.7712
10.	**PCA**	0.0266	0.9587	8.8619	5.4402	0.7990
11.	**MAX**	0.0205	0.9547	9.2181	5.8521	0.7666
12.	**AV**	0.0270	0.9626	8.8379	5.3814	0.7978
13.	**Proposed**	0.0401	0.9466	11.0998	6.3146	0.7996

Later, table 10 also demonstrates the comparisons between other standard methods [12] and our proposed image fusion method. In this table, we have shown comparisons in terms of Average Gradient (AG), Edge Retention, Figure definition (FD), QAB/F, Cross-Entropy (CE), Mutual Information (MI), Cross-Entropy (CE), Relatively Warp (RW), Edge-Intensity (EI) and Structural Similarity (SSIM). These other standard image fusion methods are Morphological Pyramid method (MP), Ratio Pyramid method (RP), Laplacian Pyramid method (LP), DWT-based method (DWT), average-based method (AV), Select maximum based method (Max), PCA-based method (PCA), Contrast Pyramid method (CP), FSD Pyramid method (FSD) and Gradient Pyramid method (GP). After analyzing the performance of our proposed method in table 9 and 10 we can say that the proposed methods in producing satisfactory results. Simultaneously, in table 9 we can see that the PSNR value achieved through the proposed method is better than other methods. Further, we have also compared our proposed image integration technique with the Singh et al. [10] and our method has shown comparable performances as compared to their method. Here, figure 7 shows the visual comparison between our suggested technique and Sing's technique.

(a) (b) (c) (d)

Fig. 8. Image fusion result comparison on Clock image set (a) Parent image 1 (b) Parent image 2 (c) Singh et al. (d) Proposed technique.

5 Conclusions

In this work, the authors have suggested a novel multi-scale image fusion scheme which uses the different edge detection kernels to generate detailed gray-scale edge map. Initially, we have used robust point matching based image registration scheme followed by NLAD process on a registered gray-scale parent image. Later, we have used four different edge detection kernels to preserve the local structure of the noise free image and to enhance the edges, boundaries and texture of the image. This approach will generate a gray-scale detailed edge map. Later, we have proposed an adaptive weight map generation scheme based on the neighboring pixels values. This weight map will give the uniqueness and importance of each and every pixel of any parent image. Finally, we have employed the winner-take-all approach which used parent image weight maps to generate final fully focused fused image. We have also carried out different image fusion experiments on two standard image datasets and the results are satisfactory. These experimental results have also shown better PSNR values as compared to the other state-of-arts methods.

References

1. Xiaoqing Luo, Zhancheng Zhang, Cuiying Zhang, and Xiaojun Wu. Multi-focus image fusion using hosvd and edge intensity. *Journal of Visual Communication and Image Representation*, 45:46 – 61, 2017.
2. Xiangzhi Bai, Yu Zhang, Fugen Zhou, and Bindang Xue. Quadtree-based multi-focus image fusion using a weighted focus-measure. *Information Fusion*, 22:105 – 118, 2015.
3. A. Ardeshir Goshtasby. Fusion of multifocus images to maximize image information, 2006.
4. Wei Huang and Zhongliang Jing. Evaluation of focus measures in multi-focus image fusion. *Pattern Recognition Letters*, 28(4):493 – 500, 2007.
5. Gemma Piella. A general framework for multiresolution image fusion: from pixels to regions. *Information Fusion*, 4(4):259 – 280, 2003.
6. Xiaoyan Luo, Jun Zhang, and Qionghai Dai. A regional image fusion based on similarity characteristics. *Signal Processing*, 92(5):1268 – 1280, 2012.
7. Shutao Li and Bin Yang. Multifocus image fusion by combining curvelet and wavelet transform. *Pattern Recognition Letters*, 29(9):1295 – 1301, 2008.
8. D. Looney and D. P. Mandic. Multiscale image fusion using complex extensions of emd. *IEEE Transactions on Signal Processing*, 57(4):1626–1630, April 2009.
9. Mansour Nejati, Shadrokh Samavi, Nader Karimi, S.M. Reza Soroushmehr, Shahram Shirani, Iman Roosta, and Kayvan Najarian. Surface area-based focus criterion for multi-focus image fusion. *Information Fusion*, 36:284 – 295, 2017.
10. Vinay Kumar Harbinder Singh and Sunil Bhooshan. Anisotropic diffusion for details enhancement in multiexposure image fusion. *ISRN Signal Processing*, 2013:1–18, 2013.
11. Larry S. Davis. A survey of edge detection techniques. *Computer Graphics and Image Processing*, 4(3):248 – 270, 1975.
12. Zhaodong Liu, Yi Chai, Hongpeng Yin, Jiayi Zhou, and Zhiqin Zhu. A novel multi-focus image fusion approach based on image decomposition. *Information Fusion*, 35:102 – 116, 2017.